ATLAS PUB Note
ATL-PHYS-PUB-2025-004
28th February 2025

# Projected sensitivity of searches for Higgs boson pair production in final states with light leptons, taus, and photons with the ATLAS detector at the HL-LHC

The ATLAS Collaboration

A projection of the sensitivity to non-resonant Higgs boson pair production in the $bbZZ$, $4V$ ($V = W$ or $Z$), $VV\tau\tau$, $4\tau$, $\gamma\gamma VV$ and $\gamma\gamma\tau\tau$ decay channels from LHC Run 2 to the High Luminosity LHC with the upgraded ATLAS detector is presented. Sensitivities are projected assuming a centre-of-mass energy of 14 TeV for integrated luminosities ranging from 1000 to 3000 $\text{fb}^{-1}$ and for a variety of systematic uncertainty scenarios. Under the baseline (statistical only) extrapolation scenario for an integrated luminosity of 3000 $\text{fb}^{-1}$, a combined signal significance of $1.0\sigma$ ($1.2\sigma$) is expected, while the 95% confidence-level upper limit on the $HH$ signal strength is found to be 2.1 (1.7). The modifier of the trilinear Higgs boson self-coupling, $\kappa_\lambda$, is correspondingly constrained to the interval [-0.8, 5.6] ([-0.6, 5.5]) at the 95% confidence level.

# 1 Introduction

Following the observation of the Higgs boson ($H$) by the ATLAS and CMS experiments at the CERN Large Hadron Collider (LHC) in 2012 [1, 2], major efforts from both Collaborations have been carried out with the aim of studying its properties in detail. From the confirmation of the Higgs boson's spin and CP nature [3, 4] to its coupling with vector bosons and third generation fermions [5–14], large portions of the Standard Model (SM) Higgs sector have been extensively explored. So far, all experimental measurements performed by ATLAS are consistent with SM predictions [15].

In the Brout-Englert-Higgs mechanism [16–18], a scalar Higgs potential $V(H)$ that spontaneously breaks the electroweak gauge symmetry is postulated, thereby generating masses of the heavy vector bosons and, through additional Yukawa couplings, the massive fermions [19]. After spontaneous symmetry breaking, the SM Higgs potential takes the form of

$$V(H) = \frac{1}{2}m_H^2 H^2 + \lambda v H^3 + \frac{1}{4}\lambda H^4 \quad ,$$

where $H$ is the Higgs field, $m_H$ is the Higgs boson mass, $v$ is the vacuum expectation value, and $\lambda$ is the Higgs self-coupling. In the SM, the value of $\lambda$ is related to $m_H$ and $v$ by $\lambda_{\text{SM}} = m_H^2/(2v^2)$. The precise measurement of this parameter would therefore provide constraints on the shape of the Higgs potential and offer an important test of the electroweak symmetry breaking mechanism. Deviations of the Higgs self-coupling from the predicted SM value play a pivotal role in many Beyond Standard Model (BSM) theories, including for example Electroweak Baryogenesis [20]. Such studies are typically performed within the $\kappa$ framework [21], also used in this note, in which coupling deviations are expressed as ratios with respect to the SM prediction, e.g. $\kappa_\lambda = \lambda/\lambda_{\text{SM}}$.

Direct measurements of $\kappa_\lambda$ involve searches for Higgs boson pair production ($HH$), which has a cross section around 1000 times smaller than that of single Higgs production. Under the operation of the LHC during its second run (Run 2) with a centre-of-mass energy of $\sqrt{s} = 13\,\text{TeV}$, the dominant $HH$ production mode is expected to be gluon-gluon fusion (ggF), with a cross-section of $31.1^{+2.1}_{-7.2}$ fb [22–29], followed by vector boson fusion (VBF), with a cross-section of $1.73 \pm 0.04$ fb [30–34]. The VBF production is additionally sensitive to the coupling between two heavy vector bosons $V$ and two Higgs bosons, $g_{HHVV}$, parameterised by the coupling modifier $\kappa_{2V}$ in the $\kappa$ framework.

The search for $HH$ production by the ATLAS Collaboration is ongoing. The latest results utilise the full Run 2 dataset and include searches in $b\bar{b}b\bar{b}$ [35, 36], $b\bar{b}\gamma\gamma$ [37], $b\bar{b}\tau^+\tau^-$ [38], multilepton [39] and $b\bar{b}\ell\ell + E_{\text{T}}^{\text{miss}}$ [40] final states. A combination of all the Run 2 searches has recently been performed [41], limiting the $HH$ signal strength at the 95% confidence level (CL) to be less than 2.9 times the SM prediction, with the expected value being 2.4, in the absence of $HH$ production. This translates into observed (expected) 95% confidence intervals for the Higgs boson self couplings of $\kappa_\lambda \in [-1.2, 7.2]$ ($[-1.6, 7.2]$) and $\kappa_{2V} \in [0.6, 1.5]$ ($[0.4, 1.6]$).

Given the small $HH$ production cross-section, all $HH$ searches are currently limited by the available size of the proton–proton collision dataset. However, this situation is expected to improve significantly during the upcoming High Luminosity phase of the LHC (HL-LHC), set to begin operation in 2030 and run until the early 2040s, in which ATLAS and CMS are expected to collect ten times more data than what has been collected in Run 2 and Run 3 so far. The HL-LHC will also operate at a centre-of-mass energy $\sqrt{s} = 14\,\text{TeV}$. In order to achieve this unprecedented milestone, the instantaneous luminosity delivered to the experiments will be increased up to $7.5 \times 10^{34}\,\text{cm}^{-2}\text{s}^{-1}$, with a peak number of $pp$ interactions per

bunch-crossing (i.e. event pile-up) of up to 200. To cope with these conditions, the ATLAS detector will be significantly upgraded. This includes the replacement of the current inner detector by a new all-silicon Inner Tracker (ITk), which will extend the $|\eta|$ coverage up to $|\eta| < 4$ [42, 43], and the addition of an entirely new High-Granularity Timing Detector [44] in the forward region, as well as upgrades to the calorimeter and muon system electronics and the trigger and data acquisition system [45–47]. This study assumes that the performance of the ATLAS detector after its HL-LHC upgrades will maintain at least the same level of performance as in Run 2, despite the challenges posed by increased pile-up. This assumption is backed by recent detector performance studies [48, 49].

This note presents a first HL-LHC projection by ATLAS of the $HH \rightarrow$ multilepton final states based on the results from Run 2 [39], assuming different luminosity scenarios from 1000 to 3000 fb$^{-1}$ at a centre-of-mass energy of $\sqrt{s} = 14$ TeV. The purpose of this note is to provide input for the 2025 update of the European Strategy for Particle Physics. The previous strategy document, published in 2019, featured the $HH$ projection results but did not include the multilepton analysis [50]. Section 2 provides a brief overview of the Run 2 analysis, while section 3 offers a detailed description of the extrapolation procedure. The results are presented in section 4 and the note concludes in section 5.

## 2 Run 2 $HH \rightarrow$ multilepton analysis

A search for Higgs boson pair production targeting multilepton final states was performed by the ATLAS Collaboration using data collected during the complete Run 2 period, with a centre-of-mass energy of $\sqrt{s} = 13$ TeV and an average of 34 $pp$ interactions per bunch-crossing. The total integrated luminosity of the dataset was $140.1 \pm 1.2$ fb$^{-1}$, recorded from 2015 to 2018 [51]. Full details of this analysis can be found in Ref. [39].

The search targeted the $HH$ process in final states with multiple light leptons and hadronically decaying taus, and in diphoton final states with one or two additional light leptons and/or hadronic taus ($\tau_{\text{had}}$). Events from $HH$ decays were selected where $H \rightarrow WW$, $ZZ$, $\tau\tau$, and $\gamma\gamma$, and a dedicated search was performed in $HH \rightarrow bbZZ$, where both $Z$ bosons decay into light leptons. Channels including $H \rightarrow \gamma\gamma$ decay were classified as the diphoton plus multilepton channels ($\gamma\gamma$+ML) while those without photons were classified as the multilepton (ML) channels. A visualisation of the final states covered in this analysis is shown in Figure 1.

Monte Carlo (MC) simulations were used to model both the signal and background processes. The dominant background to the ML channels was diboson ($VV$) production. This background was estimated from simulation and normalised to data in control regions. Data-driven methods were used to estimate background processes involving non-prompt leptons, leptons with a wrongly assigned charge, and misidentified hadronic taus. The $4l + bb$ channel also had substantial contributions from top quark pair production ($t\bar{t}$). Non-resonant $\gamma\gamma$ production was the dominant background in the $\gamma\gamma$+ML channels. The components of this $\gamma\gamma$-continuum background include $\gamma\gamma$ production in association with jets ($\gamma\gamma$ + jets), a top quark pair ($t\bar{t}\gamma\gamma$), or a vector boson ($V\gamma\gamma$). Single Higgs boson production was a background to all channels and was significant for the $4l + bb$ and $\gamma\gamma$+ML channels, with the dominant source to most channels being Higgs boson production in association with a vector boson ($VH$).

Electrons, muons, hadronic taus, photons, jets (including those containing $b$-hadrons), and missing transverse energy ($E_{\text{T}}^{\text{miss}}$) were used in this search. Electrons and muons were reconstructed from inner detector tracks. Visible hadronic tau candidates ($\tau_{\text{had-vis}}$) are reconstructed from anti-$k_t$ jets ($R = 0.4$),

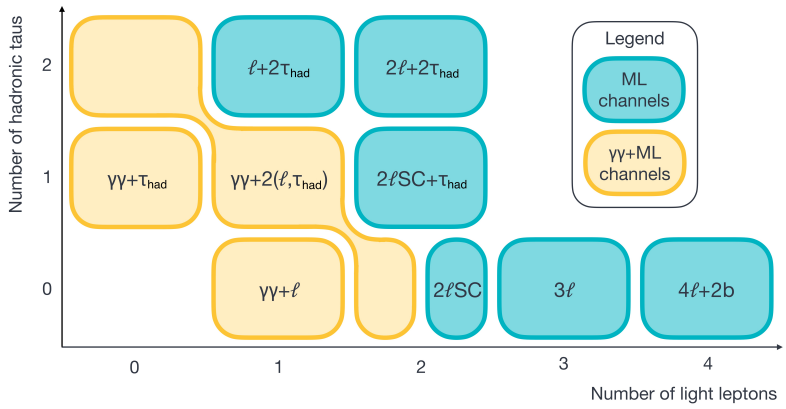


Figure 1: A visualisation of the different final states included in this analysis. The $\gamma\gamma$+ML channels are shown in the lighter yellow boxes and the ML channels are indicated by the darker turquoise boxes. 'SC' indicates that the two leptons are required to have the same charge. In the $2\ell$+$2\tau_{\text{had}}$ and $\ell$+$2\tau_{\text{had}}$ channels, the two hadronic taus are required to have opposite charges ('OC'), as are the two light leptons in the $2\ell$+$2\tau_{\text{had}}$ channel. The $\gamma\gamma$+$2(\ell, \tau_{\text{had}})$ channel requires the presence of two OC light leptons or hadronic taus in addition to the two photons, i.e. encompassing $\gamma\gamma + \ell\ell$, $\gamma\gamma + \ell\tau_{\text{had}}$, and $\gamma\gamma + \tau_{\text{had}}\tau_{\text{had}}$ signatures. Taken from Ref. [39].

required to have $p_T > 20$ GeV, $|\eta| < 2.5$, and one or three associated tracks. Their identification uses boosted decision trees (BDTs) and recurrent neural networks (RNNs), achieving efficiencies of 60-85%. Photons were required to have $E_{\text{T}} > 25$ GeV and $|\eta| < 2.37$, excluding the calorimeter transition region $1.37 < |\eta| < 1.52$. Jets were reconstructed using the anti-$k_t$ algorithm with a radius parameter $R = 0.4$ and were required to have $p_{\text{T}} > 25$ GeV and to be within $|\eta| < 2.5$ (extended to $|\eta| < 4.4$ for channels with photons). Jets containing $b$-hadrons, $b$-jets, were identified using the DL1r tagging algorithm [52] with a working point corresponding to a 77% $b$-tagging efficiency. The missing transverse energy $E_{\text{T}}^{\text{miss}}$ was calculated as the magnitude of the negative vector sum of the transverse momenta of all selected and calibrated physics objects in an event, including an additional soft term.

Events in the ML channels that have final states containing two or more light leptons were selected by requiring that they satisfy single lepton or dilepton triggers. Events in the $l + 2\tau_{\text{had}}$ channel were selected using only the single lepton triggers. Diphoton triggers where the leading (subleading) photon was required to have $E_{\text{T}} > 35$ GeV (25 GeV) were used in the $\gamma\gamma$+ML channels. After applying the overlap removal procedure, events were categorised into sub-channels according to the number of photons, $\tau_{\text{had-vis}}$, and light leptons. Each channel had its own requirements that define the signal preselection regions. These requirements also formed the basis for defining control and validation regions to estimate background contributions.

All channels except the $\gamma\gamma + 2(l, \tau_{\text{had}})$ channel used BDTs with the Gradient Boost algorithm [53] to separate signal from background processes. BDTs were used for signal background discrimination and were optimised separately for each channel, in terms of the input variables and hyperparameters, using the area under the receiver operating characteristic (ROC) curve as the performance metric. The BDT output score was used as a final discriminant in the ML channels. In the $\gamma\gamma$+ML channels, different signal regions (SRs) were defined based on the BDT score, after which a fit was performed to the $m_{\gamma\gamma}$.

For every channel, the total uncertainty was dominated by the statistical uncertainty in the number of data

events in the signal region. Experimental sources of systematic uncertainty due to the detector response and background modelling were considered, as were theoretical uncertainties in the normalisation and shape of signal and background processes. The finite statistics of MC simulations used in the analysis were also considered a source of systematic uncertainty. Experimental uncertainties due to the luminosity, trigger, reconstruction, identification and isolation efficiencies of electrons, muons, and photons were considered. Theoretical uncertainties linked to background, parton shower, and cross-section modelling, and PDF uncertainties were considered. An additional 100% theoretical uncertainty is assigned to the single Higgs production processes (ggF, VBF, and $VH$) in the $4l + 2b$ channel in order to account for difficulties in the modelling of these processes in association with heavy-flavour jets.

Measurements of the $HH$ signal strength and constraints on the self-coupling strength were obtained using a binned likelihood function, which fits the discriminating variable in each channel - the BDT output score distribution for each of the ML channels and $m_{\gamma\gamma}$ for the $\gamma\gamma$+ML channels [54]. Theoretical uncertainties in simulated signal and background processes were treated as correlated across all channels, as well as experimental uncertainties related to the data-taking conditions and physics objects. Uncertainties related to background estimates using data-informed methodologies (derived from template fits, or estimated in control or side-band data regions) were treated as uncorrelated, except in cases where a common control region (CR) was used in which case it was treated as correlated.

No significant excess over the background was observed. The overall combination yielded an observed 95% CL upper limit on $\mu_{HH}$ of 17, with an expected upper limit of 11 in the absence of $HH$ production, and 12 assuming SM $HH$ production. $3l$ and $\gamma\gamma + l$ were the most sensitive channels in the $\mu_{HH}$ upper limit. The Higgs self-coupling strength modifier, $\kappa_\lambda$ was observed (expected) to be constrained to be $-6.2 \leq \kappa_\lambda \leq 11.6$ ($-4.5 \leq \kappa_\lambda \leq 9.6$), with a best-fit value of 7.4, all at 95% CL with other couplings fixed to their SM values. $4l + bb$ was the most sensitive channel in $\kappa_\lambda$. The sensitivity of the results in all channels was limited by the statistical precision on the available data.

This analysis is used as input to the extrapolation presented in this note. The analysis strategy is unchanged and the BDTs optimised to separate signals from backgrounds in the Run 2 analysis were not retrained for HL-LHC conditions.

## 3 Extrapolation procedure

The statistical framework based on the profile likelihood ratio [55] deployed for the Run 2 results [39] is extended by scaling the signal and background expectations of the final fit discriminants, i.e the BDT output score distribution for each of the ML channels and $m_{\gamma\gamma}$ for the $\gamma\gamma$+ML channels, in each region. Under this prescription, the BDT trainings and histogram binnings are left unchanged. These extrapolations therefore likely represent a conservative result as more advanced multivariate analysis techniques utilising larger datasets, and binning strategies optimised to the larger dataset, could be exploited in the future. Final results are obtained using the asymptotic formulae [55], and upper limits on the signal strength and $\kappa_\lambda$ are set following the CLs prescription [56].

A common scale factor of $L'/L$ is applied to all signal and background processes to reflect the increase in integrated luminosity $L'$ with respect to the Run 2 luminosity of $L = 140\,\text{fb}^{-1}$. Values of $L'$ between $1000\,\text{fb}^{-1}$ and $3000\,\text{fb}^{-1}$ are considered in this study. Additionally, process-dependent scale factors are applied to account for differences in the inclusive cross-section between the Run 2 centre-of-mass energy of $\sqrt{s} = 13$ TeV and the $\sqrt{s} = 14$ TeV assumed during HL-LHC operation. The $HH$ signal and single-Higgs

background cross-sections are all scaled following the recommendations from the LHC Higgs Working Group [57]. For remaining backgrounds, a scale factor of 1.18 is applied to account for the cross-section increase arising from the enhanced gluon-luminosity, following the same assumptions as in previous projections [50]. These process-dependent scale factors are summarised in Table 1.

Table 1: Scale factors applied to the $HH$ signal and background processes to account for the change in cross-sections due to the increase of centre-of-mass energy from $\sqrt{s}$ = 13 TeV to $\sqrt{s}$ = 14 TeV at the HL-LHC, assuming a $m_H$ of 125 GeV.

| **Process** | **Scale factor** |
|---|---|
| **Signals** | |
| ggF $HH$ | 1.18 |
| VBF $HH$ | 1.19 |
| **Backgrounds** | |
| ggF $H$ | 1.13 |
| VBF $H$ | 1.13 |
| $WH$ | 1.10 |
| $ZH$ | 1.12 |
| $ttH$ | 1.21 |
| Others | 1.18 |

The signal and background expectations are scaled from the predictions obtained from the profile likelihood fit to data in the Run 2 analysis. Since many of these scale factors derived in control regions to correct for the normalisations of the backgrounds were found to deviate significantly from unity, background processes that were estimated using simulation and normalised to data in control regions are scaled by their corresponding Run 2 scale factors. This includes normalisation factors for prompt and non-prompt leptons. For backgrounds estimated entirely from data, the Run 2 projection is scaled to $L'$ with cross-section corrections applied.

Since the exact evolution of the systematics in the future can't be known with certainty, four separate scenarios are considered in this study in order to provide an envelope for interpreting the results. One general assumption made is that the performance of the ATLAS detector after its HL-LHC upgrades, in particular regarding the increased background from the higher event pile-up, is at least as good as the performance during Run 2. This is supported by current detector performance studies [48, 49]. The four systematic uncertainty scenarios are:

**Run 2 systematic uncertainties** This is the most conservative scenario, with all Run 2 systematic uncertainties left unchanged.

**Theoretical uncertainties halved** In this scenario, all theoretical uncertainties associated with the signal and background processes are scaled down by 50%. Experimental uncertainties remain at their Run 2 values.

**Baseline systematic uncertainties** This scenario represents the current baseline recommendations for HL-LHC projection studies [58], facilitating the comparison between ATLAS and CMS. The statistically limited components of the experimental uncertainties are scaled down with the square root of the integrated luminosity, while sources dominated by intrinsic detector limitations either remain constant or are scaled down taking into account the detector upgrades and improvements in analysis techniques associated with the larger available dataset. A detailed breakdown of scale factors applied in this scenario is shown in Table 2. Theoretical uncertainties are halved as described above. Statistical uncertainties on the background estimates from simulation and uncertainties in the background normalisation factors are assumed to be negligible. Uncertainties related to electrons, muons, jets and $E_{\mathrm{T}}^{\mathrm{miss}}$ remain at their Run 2 values. The $b$-tagging uncertainties for $b$- and $c$-jets are halved, while those for light-jets are kept at Run 2 levels. The photon systematic uncertainties remain at their Run 2 values, except for the photon efficiency uncertainties, which are scaled by a factor of 0.8. This scale factor corresponds to expected improvements in the methodology and, to some extent, the increased dataset available. The statistical components of the $\tau_{\mathrm{had}}$ reconstruction and identification efficiency, as well as the energy scale are scaled to zero, their systematic components are kept the same as for Run 2. The statistical components of the fake-$\tau_{\mathrm{had}}$ estimation are scaled by a factor $\sqrt{L/L'}$, while the systematic components are kept at the Run 2 levels.

Table 2: Summary of HL-LHC scale factors for the relevant experimental and theoretical systematic uncertainties defining the baseline scenario. The uncertainty labeled as 'spurious signal' accounts for potential bias associated with the choice of functional form to model the continuum background in the $\gamma\gamma$+ML channels.

| Uncertainty Source | Scale Factor |
|---|---|
| **Experimental uncertainties** | |
| Luminosity | 1.0 |
| Electrons and muons efficiency | 1.0 |
| Electron reconstruction and identification | 1.0 |
| Photon efficiency (ID, trigger, isolation efficiency) | 0.8 |
| Photon energy scale and resolution | 1.0 |
| $b$-jet $b$-tagging efficiency | 0.5 |
| $c$-jet $b$-tagging efficiency | 0.5 |
| Light jet $b$-tagging efficiency | 1.0 |
| Jet energy scale and resolution, $E_T^{\mathrm{miss}}$ | 1.0 |
| $\tau_{\mathrm{had}}$ efficiency (statistical) | 0.0 |
| $\tau_{\mathrm{had}}$ efficiency (systematic) | 1.0 |
| $\tau_{\mathrm{had}}$ energy scale | 1.0 |
| **Background modelling** | |
| Spurious signal | 0.0 |
| Fake $\tau_{\mathrm{had}}$ estimation (statistical) | $\sqrt{L/L'}$ |
| Fake $\tau_{\mathrm{had}}$ estimation (systematic) | 1.0 |
| **Theoretical uncertainties** | 0.5 |
| **MC statistics** | 0.0 |

**No systematic uncertainties** This is the most optimistic scenario, with all systematic uncertainties removed.

# 4 Results

## 4.1 *HH* production signal strength

The expected $HH$ signal significances for individual channels are presented in Table 3. These results correspond to the extrapolation scenarios discussed above for an integrated luminosity of 3000 fb$^{-1}$, assuming SM-like $HH$ production. The 95% CL upper limits on the signal strength for the statistical combinations of the ML and $\gamma\gamma$+ML signal categories, as well as the overall combination of all channels, are shown for the baseline and no systematic uncertainty scenarios in Figure 2. In the Run 2 analysis, $3l$ was the leading multilepton channel. At the HL-LHC, the $4l + bb$ channel is projected to be the most sensitive channel, mainly due to a lower luminosity scaling for single Higgs production, its main background. As for the $3l$ channel, the dominant background is non-Higgs, which has a higher luminosity scaling. Additionally, suboptimal binning in the $3l$ channel for HL-LHC may contribute to its reduced sensitivity. Applying optimised binning across all channels would likely alter their relative sensitivities. The $\gamma\gamma$+ML channels exhibit minimal change between the systematic scenarios, as their uncertainties are predominantly driven by statistical limitations.

Table 3: Expected significance for the four extrapolation scenarios at integrated luminosity of 3000 fb$^{-1}$.

| Significance | No syst. unc. | Baseline | Theory unc. 50% | Run 2 syst. unc. |
|---|---|---|---|---|
| $4l + bb$ | 0.6 | 0.6 | 0.5 | 0.5 |
| $3l$ | 0.5 | 0.4 | 0.2 | 0.2 |
| $2l$SC | 0.3 | 0.3 | 0.1 | 0.1 |
| $2l$SC + $\tau_{\text{had}}$ | 0.2 | 0.2 | 0.1 | 0.1 |
| $2l + 2\tau_{\text{had}}$ | 0.4 | 0.4 | 0.2 | 0.2 |
| $1l + 2\tau_{\text{had}}$ | 0.3 | 0.2 | 0.1 | 0.1 |
| Combined ML | 1.0 | 0.8 | 0.6 | 0.6 |
| $\gamma\gamma + 2l$ | 0.4 | 0.4 | 0.4 | 0.4 |
| $\gamma\gamma + l$ | 0.5 | 0.4 | 0.4 | 0.4 |
| $\gamma\gamma + \tau_{\text{had}}$ | 0.2 | 0.2 | 0.2 | 0.2 |
| Combined $\gamma\gamma$+ML | 0.7 | 0.6 | 0.6 | 0.5 |
| Combined | 1.2 | 1.0 | 0.9 | 0.8 |

Table 4 presents the expected significance and the 68% CL interval on the $HH$ signal strength for $\mu_{HH} = 1$, and the expected 95% CL exclusion limits, assuming $\mu_{HH} = 0$, for each extrapolation scenario for integrated luminosities of 2000 and 3000 fb$^{-1}$. The 68% CL interval on $\mu_{HH}$ is expressed as percentage deviations from the expected value of $\mu_{HH} = 1$. The corresponding results are shown for luminosity values ranging from 1000 to 3000 fb$^{-1}$ in Figures 3(a), 3(b) and 4 respectively. The overall combination yields a signal significance of $1.0\sigma$ in the baseline scenario at an integrated luminosity of 3000 fb$^{-1}$. An expected 95% CL upper limit on $\mu_{HH}$ of 2.1 times the SM cross-section is obtained, assuming no $HH$ production. When systematic uncertainties are neglected, the expected significance increases to $1.2\sigma$, with an expected upper limit on $\mu_{HH}$ of 1.7 times the SM prediction.

Table 5 summarises the impact of different sources of uncertainty on the expected $\mu_{HH}$ upper limit at 95% CL for the baseline scenario at an integrated luminosity of 3000 fb$^{-1}$. The table presents results for the

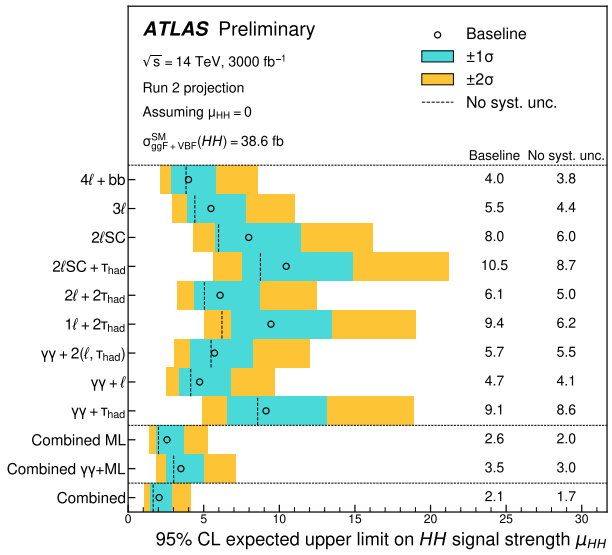


Figure 2: Expected upper limits on the $HH$ signal strength $\mu_{HH}$ assuming $\mu_{HH} = 0$ at the 95% CL at $\sqrt{s} = 14$ TeV for 3000 fb$^{-1}$ under the baseline scenario, together with the numerical values for the scenario with no systematic uncertainties. The $\pm1\sigma$ and $\pm2\sigma$ bands shown in the legend correspond to the baseline scenario. Results are presented individually for the different search channels, the statistical combination of ML and $\gamma\gamma$+ML channels separately, and the statistical combination of all channels.

Table 4: Expected 95% CL upper limit, $HH$ signal significance, and 68% CL interval for $\mu_{HH} = 1$ under each uncertainty scenario at integrated luminosities of 2000 fb$^{-1}$ and 3000 fb$^{-1}$ for the full multilepton combination.

| **Extrapolation scenario** | **95% CL upper limit** [assuming $\mu_{HH} = 0$] | **Significance [$\sigma$]** [assuming $\mu_{HH} = 1$] | **68% CL interval on $\mu_{HH}$ [%]** |
|---|---|---|---|
| $L_{\text{int}} = 2000\,\text{fb}^{-1}$ | | | |
| Run 2 syst. unc. | 3.3 | 0.7 | -144 / +161 |
| Theory unc. 50% | 2.8 | 0.7 | -134 / +140 |
| Baseline | 2.5 | 0.8 | -115 / +121 |
| No syst. unc. | 2.0 | 1.0 | -100 / +103 |
| $L_{\text{int}} = 3000\,\text{fb}^{-1}$ | | | |
| Run 2 syst. unc. | 2.9 | 0.8 | -126 / +140 |
| Theory unc. 50% | 2.4 | 0.9 | -116 / +122 |
| Baseline | 2.1 | 1.0 | -96 / +100 |
| No syst. unc. | 1.7 | 1.2 | -83 / +84 |

combination of all channels, as well as separately for the combinations of the ML channels and the $\gamma\gamma$+ML channels.

The expected signal significance for $HH$ production is also estimated for cases where the Higgs boson self-coupling deviates from its SM prediction, i.e., $\kappa_\lambda \neq 1$. Figure 5 shows this for a target luminosity of 3000 fb$^{-1}$ across the different extrapolation scenarios considered in this note.

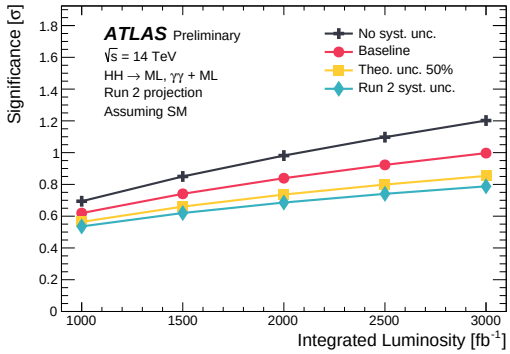


(a) Significance

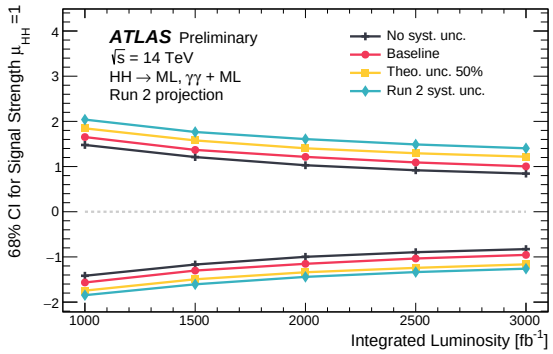


(b) 68% confidence interval for $\mu_{HH} = 1$

Figure 3: (a) Expected $HH$ signal significance for the signal strength $\mu_{HH} = 1$ as a function of luminosity. (b) Expected 68% confidence interval for the $HH$ signal strength. Results are provided for each of the extrapolation scenarios described in the text.

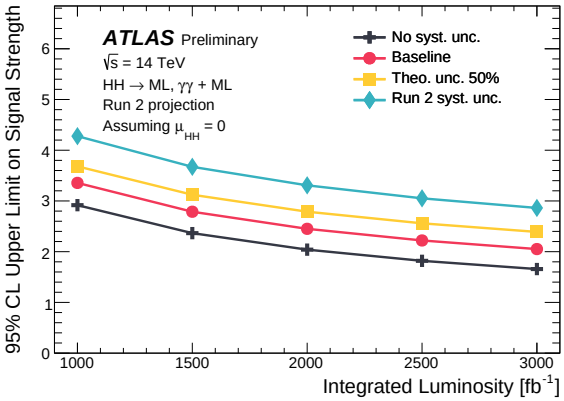


Figure 4: Expected upper limit on the $HH$ signal strength $\mu_{HH}$ assuming $\mu_{HH} = 0$ at the 95% CL as a function of various integrated luminosities from 1000 fb$^{-1}$ to 3000 fb$^{-1}$ at $\sqrt{s} = 14$ TeV for each of the extrapolation scenarios described in the text.

Table 5: Breakdown of the relative contributions to the baseline scenario uncertainties in the expected $\mu_{HH}$ upper limit at 95% CL for combinations of the ML channels, the $\gamma\gamma$+ML channels, and all channels for the baseline scenario at an integrated luminosity of 3000 fb$^{-1}$. The impact of a particular source of uncertainty is quantified as the relative variation of the expected upper limit when re-evaluating the profile likelihood ratio after fixing the corresponding nuisance parameters to their best-fit values, while all other nuisance parameters are allowed to float. The impact of data statistics is evaluated through the ratio of the expected upper limit when fixing all nuisance parameters to their best-fit values over the expected upper limit when allowing all nuisance parameters to float. Individual sources of uncertainty with an impact smaller than 1% in all channels are not listed.

| Systematic uncertainty source | Relative impact of systematic uncertainties [%] | | |
|---|---|---|---|
| | ML channels | $\gamma\gamma$+ML channels | Combination |
| **Data Statistics** | 75 | 81 | 75 |
| **Total Systematics** | **23** | **19** | **24** |
| **Experimental** | 10 | <1 | 7 |
| Detector Response | 8 | <1 | 6 |
| Jet and $E_{\mathrm{T}}^{\mathrm{miss}}$ | 4 | | 3 |
| Flavour Tagging | 2 | | 1 |
| Background Estimation | 3 | <1 | 2 |
| Prompt Lepton | 1 | | 1 |
| Non-Prompt Lepton | 1 | | 1 |
| **Theoretical** | 8 | 19 | 14 |
| Signal | 2 | 3 | 3 |
| Backgrounds | 6 | 16 | 11 |
| Single Higgs | 5 | 16 | 11 |

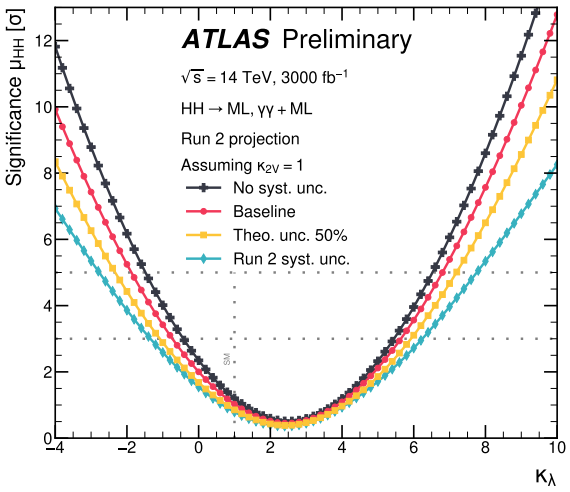


Figure 5: Expected $HH$ significance assuming different values of $\kappa_\lambda$ for 3000 fb$^{-1}$ at $\sqrt{s} = 14$ TeV for the extrapolation scenarios described in the text. The dashed horizontal lines indicate the threshold to claim the evidence ($3\sigma$) and the observation ($5\sigma$). The dashed vertical line indicates the SM hypothesis with $\kappa_\lambda = 1$.

### 4.2 Constraints on $\kappa_\lambda$

The combined expected values of twice the negative-logarithm of the profile likelihood ratio of $\kappa_\lambda$ are shown in Figure 6(a) for 3000 fb$^{-1}$, while the expected 68% and 95% confidence intervals for $\kappa_\lambda$ are shown in Table 6 for 2000 and 3000 fb$^{-1}$ under the four extrapolation scenarios. The constraints on the Higgs self-coupling strength are calculated with all other parameters fixed at their SM values. Figure 6(b) presents the constraints on $\kappa_\lambda$ for the ML and $\gamma\gamma$+ML channels separately, as well as their statistical combination for the baseline scenario at an integrated luminosity of 3000 fb$^{-1}$.

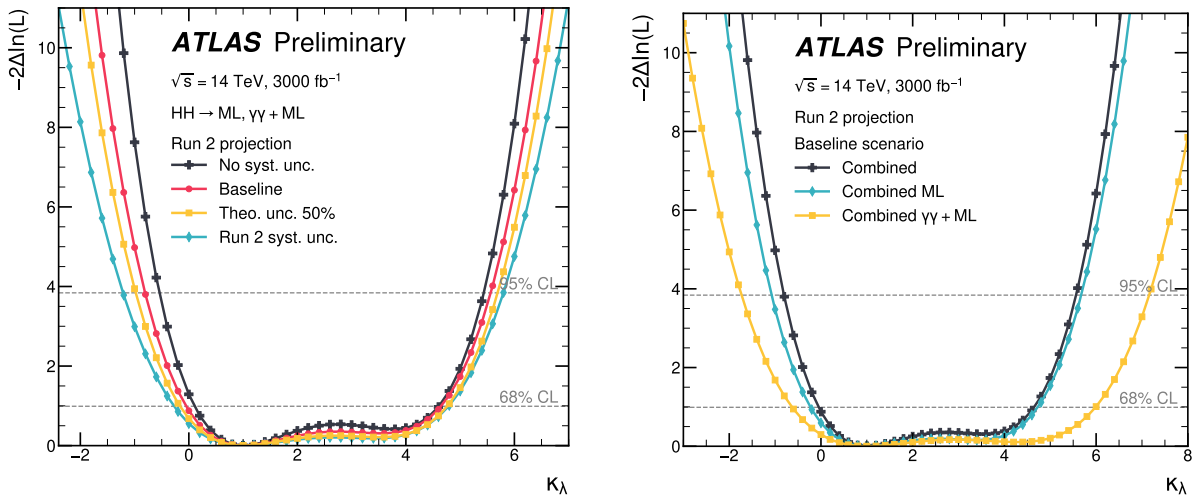


(a) (b)

Figure 6: Expected values of the negative log-likelihood ratio as a function of $\kappa_\lambda$ with the Asimov dataset generated under the SM hypothesis ($\kappa_\lambda = 1$), for (a) different systematic uncertainty scenarios and (b) ML and $\gamma\gamma$+ML channels separately as well as their combination under the baseline scenario at an integrated luminosity of 3000 fb$^{-1}$.

Table 6: Expected confidence intervals at 68% and 95% confidence levels for $\kappa_\lambda$ at 2000 and 3000 fb$^{-1}$ at $\sqrt{s} = 14$ TeV for four extrapolation scenarios.

| | **68% Confidence Interval on $\kappa_\lambda$** | | **95% Confidence Interval on $\kappa_\lambda$** | |
|---|---|---|---|---|
| **Extrapolation scenario** | 2000 fb$^{-1}$ | 3000 fb$^{-1}$ | 2000 fb$^{-1}$ | 3000 fb$^{-1}$ |
| Run 2 syst. unc. | [-0.4, 5.0] | [-0.3, 4.8] | [-1.5, 6.1] | [-1.3, 5.8] |
| Theory unc. 50% | [-0.3, 5.0] | [-0.2, 4.8] | [-1.2, 6.0] | [-1.0, 5.7] |
| Baseline | [-0.2, 4.9] | [-0.1, 4.7] | [-1.1, 5.9] | [-0.8, 5.6] |
| No syst. unc. | [-0.1, 4.9] | [0.1, 4.6] | [-0.8, 5.8] | [-0.6, 5.5] |

Figure 7 displays the expected range of the 68% confidence intervals on $\kappa_\lambda$ as a function of the assumed $\kappa_\lambda$ value when generating the Asimov dataset for the four extrapolation scenarios at 3000 fb$^{-1}$.

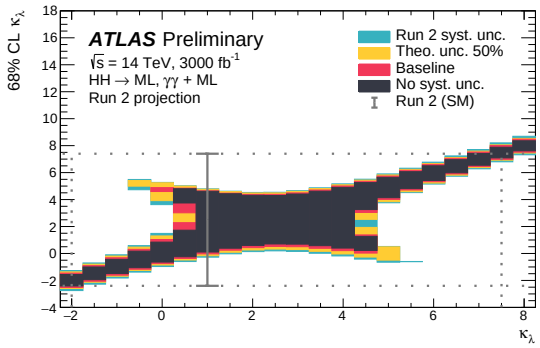


Figure 7: Expected range of the 68% confidence interval $\kappa_\lambda$ at an integrated luminosity of 3000 fb$^{-1}$ at $\sqrt{s}$ = 14 TeV as a function of the assumed $\kappa_\lambda$ value when generating the Asimov dataset for the four extrapolation scenarios. The result from the Run 2 analysis is shown in grey.

# 5 Conclusion

HL-LHC projection studies on the search for Higgs boson pair production in the $bbZZ$, $4V$ ($V = W$ or $Z$), $VV\tau\tau$, $4\tau$, $\gamma\gamma VV$ and $\gamma\gamma\tau\tau$ decay channels with the ATLAS detector are presented in this note. Several scenarios for extrapolating the systematic uncertainties from the Run 2 analysis are considered. Assuming SM-like $HH$ production, a signal significance of $1.0\sigma$ is expected in the baseline extrapolation scenario for an integrated luminosity of 3000 fb$^{-1}$, while this value increases to $1.2\sigma$ in the optimistic scenario with no systematic uncertainties. This translates into $\kappa_\lambda$ being constrained at the 95% confidence level to the interval [-0.8, 5.6] in the baseline scenario and [-0.6, 5.5] in the scenario with no systematic uncertainties. Under the background-only hypothesis, the 95% CL upper limit on the $HH$ signal strength is found to be 2.1 (1.7) for the baseline (statistical only) scenario.

# Appendix

The expected values of the negative log-likelihood ratio as a function of $\kappa_\lambda$ are shown for individual ML and $\gamma\gamma$+ML channels and their combinations in Figures 8 and 9, respectively. The Asimov dataset is generated under the SM hypothesis ($\kappa_\lambda = 1$) under the baseline scenario at an integrated luminosity of 3000 fb$^{-1}$.

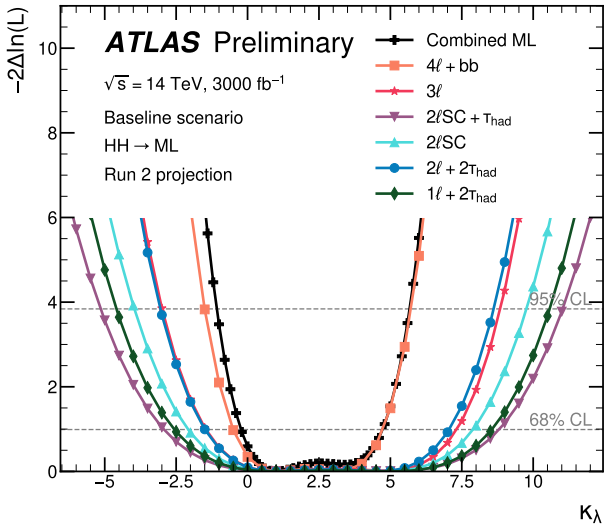


Figure 8: Expected values of the negative log-likelihood ratio as a function of $\kappa_\lambda$ with the Asimov dataset generated under the SM hypothesis ($\kappa_\lambda = 1$), for the ML channels under the baseline scenario at an integrated luminosity of 3000 fb$^{-1}$.

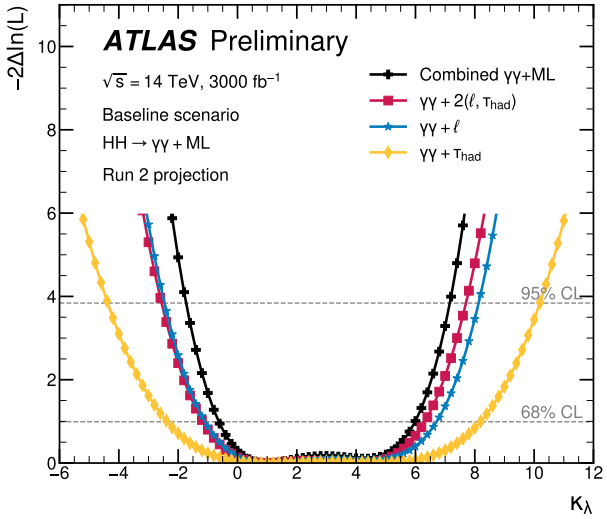


Figure 9: Expected values of the negative log-likelihood ratio as a function of $\kappa_\lambda$ with the Asimov dataset generated under the SM hypothesis ($\kappa_\lambda = 1$), for the $\gamma\gamma$+ML channels under the baseline scenario at an integrated luminosity of 3000 fb$^{-1}$.

## References


[1] ATLAS Collaboration, *Observation of a new particle in the search for the Standard Model Higgs boson with the ATLAS detector at the LHC*, Phys. Lett. B **716** (2012) 1, arXiv: 1207.7214 [hep-ex] (cit. on p. 2).

[2] CMS Collaboration, *Observation of a new boson at a mass of 125 GeV with the CMS experiment at the LHC*, Phys. Lett. B **716** (2012) 30, arXiv: 1207.7235 [hep-ex] (cit. on p. 2).

[3] ATLAS Collaboration, *Study of the spin and parity of the Higgs boson in diboson decays with the ATLAS detector*, Eur. Phys. J. C **75** (2015) 476, arXiv: 1506.05669 [hep-ex] (cit. on p. 2), Erratum: Eur. Phys. J. C **76** (2016) 152.

[4] CMS Collaboration, *Constraints on the spin-parity and anomalous HVV couplings of the Higgs boson in proton collisions at 7 and 8 TeV*, Phys. Rev. D **92** (2015) 012004, arXiv: 1411.3441 [hep-ex] (cit. on p. 2).

[5] ATLAS Collaboration, *Measurements of Higgs boson production and couplings in diboson final states with the ATLAS detector at the LHC*, Phys. Lett. B **726** (2013) 88, arXiv: 1307.1427 [hep-ex] (cit. on p. 2), Erratum: Phys. Lett. B **734** (2014) 406.

[6] CMS Collaboration, *Observation of the diphoton decay of the Higgs boson and measurement of its properties*, Eur. Phys. J. C **74** (2014) 3076, arXiv: 1407.0558 [hep-ex] (cit. on p. 2).

[7] CMS Collaboration, *Measurement of the properties of a Higgs boson in the four-lepton final state*, Phys. Rev. D **89** (2014) 092007, arXiv: 1312.5353 [hep-ex] (cit. on p. 2).

[8] ATLAS Collaboration, *Observation and measurement of Higgs boson decays to $WW^*$ with the ATLAS detector*, Phys. Rev. D **92** (2015) 012006, arXiv: 1412.2641 [hep-ex] (cit. on p. 2).

[9] CMS Collaboration, *Observation of the Higgs boson decay to a pair of $\tau$ leptons with the CMS detector*, Phys. Lett. B **779** (2018) 283, arXiv: 1708.00373 [hep-ex] (cit. on p. 2).

[10] ATLAS Collaboration, *Cross-section measurements of the Higgs boson decaying into a pair of $\tau$-leptons in proton–proton collisions at $\sqrt{s} = 13$ TeV with the ATLAS detector*, Phys. Rev. D **99** (2019) 072001, arXiv: 1811.08856 [hep-ex] (cit. on p. 2).

[11] ATLAS Collaboration, *Observation of $H \to b\bar{b}$ decays and $VH$ production with the ATLAS detector*, Phys. Lett. B **786** (2018) 59, arXiv: 1808.08238 [hep-ex] (cit. on p. 2).

[12] CMS Collaboration, *Observation of Higgs Boson Decay to Bottom Quarks*, Phys. Rev. Lett. **121** (2018) 121801, arXiv: 1808.08242 [hep-ex] (cit. on p. 2).

[13] ATLAS Collaboration, *Observation of Higgs boson production in association with a top quark pair at the LHC with the ATLAS detector*, Phys. Lett. B **784** (2018) 173, arXiv: 1806.00425 [hep-ex] (cit. on p. 2).

[14] CMS Collaboration, *Observation of $t\bar{t}H$ Production*, Phys. Rev. Lett. **120** (2018) 231801, arXiv: 1804.02610 [hep-ex] (cit. on p. 2).

[15] ATLAS Collaboration,
*A detailed map of Higgs boson interactions by the ATLAS experiment ten years after the discovery*,
Nature **607** (2022) 52, arXiv: 2207.00092 [hep-ex] (cit. on p. 2),
Erratum: Nature **612** (2022) E24.

[16] F. Englert and R. Brout, *Broken Symmetry and the Mass of Gauge Vector Mesons*,
Phys. Rev. Lett. **13** (1964) 321, ed. by J. C. Taylor (cit. on p. 2).

[17] P. W. Higgs, *Broken Symmetries and the Masses of Gauge Bosons*,
Phys. Rev. Lett. **13** (1964) 508, ed. by J. C. Taylor (cit. on p. 2).

[18] G. S. Guralnik, C. R. Hagen and T. W. B. Kibble,
*Global Conservation Laws and Massless Particles*,
Phys. Rev. Lett. **13** (1964) 585, ed. by J. C. Taylor (cit. on p. 2).

[19] S. Weinberg, *A Model of Leptons*, Phys. Rev. Lett. **19** (1967) 1264 (cit. on p. 2).

[20] D. Morrissey and M. Ramsey-Musolf, *Electroweak baryogenesis*, New J. Phys. **14** (2012) 125003,
arXiv: 1206.2942 [hep-ph] (cit. on p. 2).

[21] LHC Higgs Cross Section Working Group,
*Handbook of LHC Higgs Cross Sections: 3. Higgs Properties*,
(2013), ed. by S. Heinemeyer, C. Mariotti, G. Passarino and R. Tanaka,
arXiv: 1307.1347 [hep-ph] (cit. on p. 2).

[22] S. Dawson, S. Dittmaier and M. Spira,
*Neutral Higgs boson pair production at hadron colliders: QCD corrections*,
Phys. Rev. D **58** (1998) 115012, arXiv: hep-ph/9805244 (cit. on p. 2).

[23] S. Borowka et al., *Higgs Boson Pair Production in Gluon Fusion at Next-to-Leading Order with Full Top-Quark Mass Dependence*, Phys. Rev. Lett. **117** (2016) 012001,
arXiv: 1604.06447 [hep-ph], Erratum: Phys. Rev. Lett. 117, (2016) 079901 (cit. on p. 2).

[24] J. Baglio et al., *Gluon fusion into Higgs pairs at NLO QCD and the top mass scheme*,
Eur. Phys. J. C **79** (2019) 459, arXiv: 1811.05692 [hep-ph] (cit. on p. 2).

[25] D. de Florian and J. Mazzitelli,
*Higgs Boson Pair Production at Next-to-Next-to-Leading Order in QCD*,
Phys. Rev. Lett. **111** (2013) 201801, arXiv: 1309.6594 [hep-ph] (cit. on p. 2).

[26] D. Y. Shao, C. S. Li, H. T. Li and J. Wang,
*Threshold resummation effects in Higgs boson pair production at the LHC*, JHEP **07** (2013) 169,
arXiv: 1301.1245 [hep-ph] (cit. on p. 2).

[27] D. de Florian and J. Mazzitelli,
*Higgs pair production at next-to-next-to-leading logarithmic accuracy at the LHC*,
JHEP **09** (2015) 053, arXiv: 1505.07122 [hep-ph] (cit. on p. 2).

[28] M. Grazzini et al., *Higgs boson pair production at NNLO with top quark mass effects*,
JHEP **05** (2018) 059, arXiv: 1803.02463 [hep-ph] (cit. on p. 2).

[29] J. Baglio et al., $gg \to HH$ *: Combined uncertainties*, Phys. Rev. D **103** (2021) 056002,
arXiv: 2008.11626 [hep-ph] (cit. on p. 2).

[30] J. Baglio et al., *The measurement of the Higgs self-coupling at the LHC: theoretical status*,
JHEP **04** (2013) 151, arXiv: 1212.5581 [hep-ph] (cit. on p. 2).

[31] R. Frederix et al., *Higgs pair production at the LHC with NLO and parton-shower effects*, Phys. Lett. B **732** (2014) 142, arXiv: 1401.7340 [hep-ph] (cit. on p. 2).

[32] L.-S. Ling et al., *NNLO QCD corrections to Higgs pair production via vector boson fusion at hadron colliders*, Phys. Rev. D **89** (2014) 073001, arXiv: 1401.7754 [hep-ph] (cit. on p. 2).

[33] F. A. Dreyer and A. Karlberg, *Fully differential vector-boson fusion Higgs pair production at next-to-next-to-leading order*, Phys. Rev. D **99** (2019) 074028, arXiv: 1811.07918 [hep-ph] (cit. on p. 2).

[34] F. A. Dreyer and A. Karlberg, *Vector-boson fusion Higgs pair production at $N^3LO$*, Phys. Rev. D **98** (2018) 114016, arXiv: 1811.07906 [hep-ph] (cit. on p. 2).

[35] ATLAS Collaboration, *Search for nonresonant pair production of Higgs bosons in the $b\bar{b}b\bar{b}$ final state in $pp$ collisions at $\sqrt{s} = 13$ TeV with the ATLAS detector*, Phys. Rev. D **108** (2023) 052003, arXiv: 2301.03212 [hep-ex] (cit. on p. 2).

[36] ATLAS Collaboration, *Search for pair production of boosted Higgs bosons via vector-boson fusion in the $b\bar{b}b\bar{b}$ final state using $pp$ collisions at $\sqrt{s} = 13$ TeV with the ATLAS detector*, Phys. Lett. B **858** (2024) 139007, arXiv: 2404.17193 [hep-ex] (cit. on p. 2).

[37] ATLAS Collaboration, *Studies of new Higgs boson interactions through nonresonant $HH$ production in the $b\bar{b}\gamma\gamma$ final state in $pp$ collisions at $\sqrt{s} = 13$ TeV with the ATLAS detector*, JHEP **01** (2024) 066, arXiv: 2310.12301 [hep-ex] (cit. on p. 2).

[38] ATLAS Collaboration, *Search for the non-resonant production of Higgs boson pairs via gluon fusion and vector-boson fusion in the $b\bar{b}\tau^+\tau^-$ final state in proton–proton collisions at $\sqrt{s} = 13$ TeV with the ATLAS detector*, Phys. Rev. D **110** (2024) 032012, arXiv: 2404.12660 [hep-ex] (cit. on p. 2).

[39] ATLAS Collaboration, *Search for non-resonant Higgs boson pair production in final states with leptons, taus, and photons in $pp$ collisions at $\sqrt{s} = 13$ TeV with the ATLAS detector*, JHEP **08** (2024) 164, arXiv: 2405.20040 [hep-ex] (cit. on pp. 2–5).

[40] ATLAS Collaboration, *Search for non-resonant Higgs boson pair production in the $2b + 2\ell + E_T^{miss}$ final state in $pp$ collisions at $\sqrt{s} = 13$TeV with the ATLAS detector*, JHEP **02** (2024) 037, arXiv: 2310.11286 [hep-ex] (cit. on p. 2).

[41] ATLAS Collaboration, *Combination of Searches for Higgs Boson Pair Production in $pp$ Collisions at $\sqrt{s} = 13$ TeV with the ATLAS detector*, Phys. Rev. Lett. **133** (2024) 101801, arXiv: 2406.09971 [hep-ex] (cit. on p. 2).

[42] ATLAS Collaboration, *ATLAS Inner Tracker Pixel Detector: Technical Design Report*, ATLAS-TDR-030; CERN-LHCC-2017-021, 2017, URL: https://cds.cern.ch/record/2285585 (cit. on p. 3).

[43] ATLAS Collaboration, *ATLAS Inner Tracker Strip Detector: Technical Design Report*, ATLAS-TDR-025; CERN-LHCC-2017-005, 2017, URL: https://cds.cern.ch/record/2257755 (cit. on p. 3).

[44] ATLAS Collaboration, *A High-Granularity Timing Detector for the ATLAS Phase-II Upgrade: Technical Design Report*, ATLAS-TDR-031; CERN-LHCC-2020-007, 2020, URL: https://cds.cern.ch/record/2719855 (cit. on p. 3).

[45] ATLAS Collaboration, *ATLAS Tile Calorimeter Phase-II Upgrade: Technical Design Report*, ATLAS-TDR-028; CERN-LHCC-2017-019, 2017, URL: https://cds.cern.ch/record/2285583 (cit. on p. 3).

[46] ATLAS Collaboration, *ATLAS LAr Calorimeter Phase-II Upgrade: Technical Design Report*, ATLAS-TDR-027; CERN-LHCC-2017-018, 2017, URL: https://cds.cern.ch/record/2285582 (cit. on p. 3).

[47] ATLAS Collaboration, *ATLAS TDAQ Phase-II Upgrade: Technical Design Report*, ATLAS-TDR-029; CERN-LHCC-2017-020, 2017, URL: https://cds.cern.ch/record/2285584 (cit. on p. 3).

[48] ATLAS Collaboration, *Expected performance of the ATLAS detector at the High-Luminosity LHC*, ATL-PHYS-PUB-2019-005, 2019, URL: https://cds.cern.ch/record/2655304 (cit. on pp. 3, 6).

[49] ATLAS Collaboration, *Expected tracking and related performance with the updated ATLAS Inner Tracker layout at the High-Luminosity LHC*, ATL-PHYS-PUB-2021-024, 2021, URL: https://cds.cern.ch/record/2776651 (cit. on pp. 3, 6).

[50] ATLAS Collaboration, *Measurement prospects of the pair production and self-coupling of the Higgs boson with the ATLAS experiment at the HL-LHC*, ATL-PHYS-PUB-2018-053, 2018, URL: https://cds.cern.ch/record/2652727 (cit. on pp. 3, 6).

[51] ATLAS Collaboration, *Luminosity determination in $pp$ collisions at $\sqrt{s} = 13$ TeV using the ATLAS detector at the LHC*, Eur. Phys. J. C **83** (2023) 982, arXiv: 2212.09379 [hep-ex] (cit. on p. 3).

[52] ATLAS Collaboration, *ATLAS flavour-tagging algorithms for the LHC Run 2 $pp$ collision dataset*, Eur. Phys. J. C **83** (2023) 681, arXiv: 2211.16345 [physics.data-an] (cit. on p. 4).

[53] J. Friedman, *Greedy function approximation: A gradient boosting machine*, The Annals of Statistics **29** (2001) 1189 (cit. on p. 4).

[54] ATLAS Collaboration, *Combined search for the Standard Model Higgs boson in $pp$ collisions at $\sqrt{s} = 7$ TeV with the ATLAS detector*, Phys. Rev. D **86** (2012) 032003, arXiv: 1207.0319 [hep-ex] (cit. on p. 5).

[55] G. Cowan, K. Cranmer, E. Gross and O. Vitells, *Asymptotic formulae for likelihood-based tests of new physics*, Eur. Phys. J. C **71** (2011) 1554, arXiv: 1007.1727 [physics.data-an] (cit. on p. 5), Erratum: Eur. Phys. J. C **73** (2013) 2501.

[56] A. L. Read, *Presentation of search results: the $CL_S$ technique*, J. Phys. G **28** (2002) 2693 (cit. on p. 5).

[57] M. Cepeda et al., *Report from Working Group 2: Higgs Physics at the HL-LHC and HE-LHC*, CERN Yellow Rep. Monogr. **7** (2019) 221, ed. by A. Dainese et al., arXiv: 1902.00134 (cit. on p. 6).

[58] ATLAS and CMS Collaborations, *Addendum to the report on the physics at the HL-LHC, and perspectives for the HE-LHC: Collection of notes from ATLAS and CMS*, CERN Yellow Rep. Monogr. **7** (2019) Addendum, arXiv: 1902.10229 [hep-ex] (cit. on p. 7).